Earth Planets Space, **62**, 47–52, 2010

Scattering parameterization for interpreting asteroid polarimetric and photometric phase effects

Karri Muinonen[1], Jani Tyynelä[2], Evgenij Zubko[3,4], and Gorden Videen[5]

[1]*Observatory, P.O. Box 14, FI-00014 University of Helsinki, Finland*
[2]*Department of Physics, P.O. Box 64, FI-00014 University of Helsinki, Finland*
[3]*Center for Atmospheric and Oceanic Studies, Graduate School of Science, Tohoku University, Aoba, Aramakiaza, Aoba-ku, Sendai 980-8578, Japan*
[4]*Astronomical Institute, Kharkov National University, 35 Sumskaya Street, Kharkov 61022, Ukraine*
[5]*Army Research Laboratory, CI-ES, 2800 Powder Mill Road, Adelphi, Maryland 20783, U.S.A.*

(Received September 5, 2008; Revised January 20, 2009; Accepted January 23, 2009; Online published February 12, 2010)

We derive an analytical parameterization of the amplitude and Mueller scattering matrices of a system composed of a small number of electric dipoles. The appeal of this derivation is that it provides a wide range of light-scattering polarization states with a minimal number of parameters. Such a tool can be used to interpret observations in terms of physical parameters. We aim to utilize these results in multiple-scattering studies, such as the interpretation of polarimetric and photometric phase effects of asteroids and other atmosphereless solar-system objects.

Key words: Light scattering, coherent backscattering, photometry, polarimetry, cosmic dust, small particle, negative polarization, opposition effect.

1. Introduction

Two ubiquitous phenomena are observed near opposition for asteroids and other atmosphereless solar-system objects as well as for cometary and interplanetary dust: negative degree of linear polarization and opposition effect. The phenomena are confined to Sun-object-observer angles (phase angles) of less than 30 and 10 degrees, respectively. Sometimes they appear at extremely small phase angles, less than one degree. Negative polarization implies that the intensity polarized parallel to the Sun-object-observer plane (scattering plane) is predominating over the one perpendicular to the plane. The opposition effect is a nonlinear surge of brightness towards the backward scattering geometry. The coherent-backscattering and shadowing mechanisms have been considered as the primary causes for the phenomena.

Wide backscattering peaks and negative polarization branches have been detected consistently in extensive numerical simulations of light scattering by irregular wavelength-scale particles (e.g., Lumme and Rahola, 1998; Zubko *et al*., 2006a; Muinonen *et al*., 2007a). The phenomena are present for compact irregular particles as well as for irregular aggregates of constituent spherical or nonspherical particles. Recently, we have succeeded in uncovering internal-field characteristics that give rise to such polarization and intensity signatures (Zubko *et al*., 2006b, 2007; Muinonen *et al*., 2007a; Tyynelä *et al*., 2007, 2008; Muinonen and Erkkilä, 2007) and thus have introduced a single-scattering polarization and intensity mechanism (Muinonen *et al*., 2007b). As to the light-scattering experiments, by measuring the single-particle scattering characteristics and those of a close-packed particulate medium of similar single particles, it has been established that the particulate media continue to exhibit single-particle polarization characteristics but that these characteristics are neutralized (e.g., Shkuratov *et al*., 2004).

Multiple-scattering models for planetary surfaces depend on five groups of physical parameters. First, surface roughness in length scales of several wavelengths and large numbers of particles causes surfacial or interfacial shadowing effects. Second, the porosity of the particulate medium causes volume shadowing effects—again, the length scales are large compared to the wavelength and size of the particles. Third, particle size introduces its signature into the scattering characteristics. Fourth, particle shape plays an important role in determining the detailed structure of the scattering matrix. Fifth, the complex refractive index represents the refractory optical properties of the material of which the particles are composed.

In Section 2, we review the interference effects in scattering by multiple small scatterers essential for the present study. In Section 3, we develop scattering parameterizations based on systems composed of a small number of electric dipoles. We conclude the article in Section 4 describing future prospects for the scattering parameterization developed.

doi:10.5047/eps.2009.01.001

2. Single-scattering Interference Characteristics

In order to illustrate single-scattering interference of relevance to the present study (Muinonen *et al*., 2007a; Tyynelä

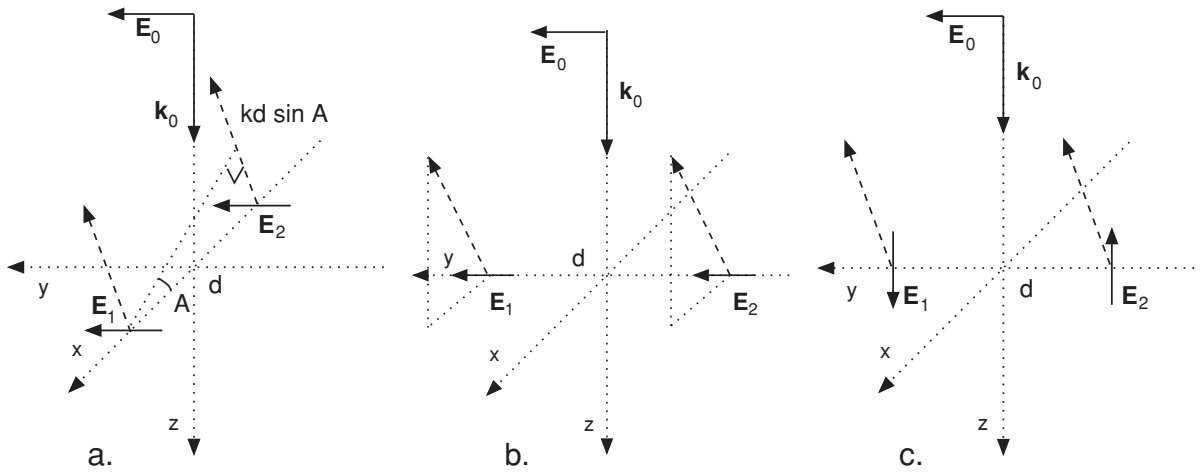

Fig. 1. Illustration of the induced internal-field components and their relation to the scattered field near the backward direction in the xz-plane for perpendicular incident polarization. See text for more details.

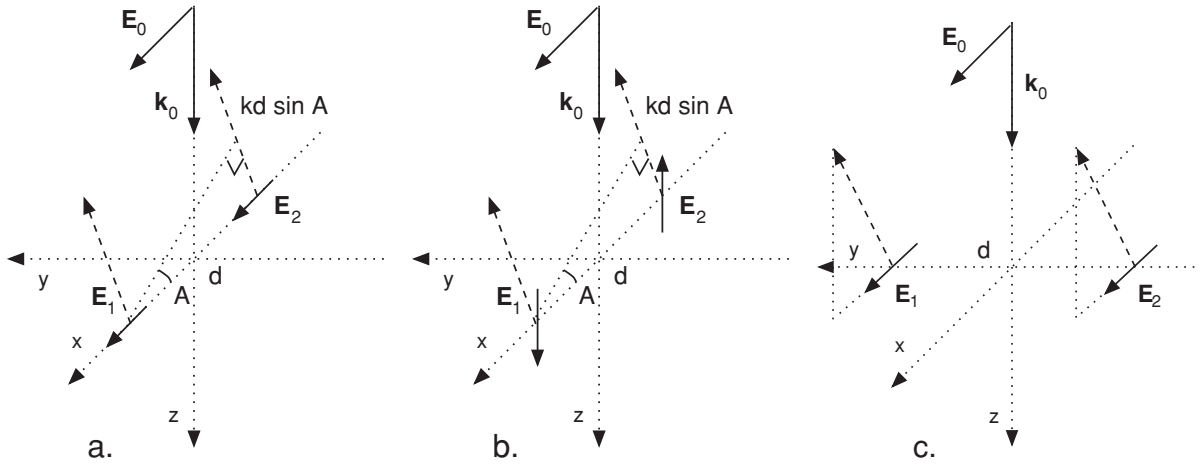

Fig. 2. As in Fig. 1 for parallel incident polarization.

et al., 2007), we consider an electromagnetic plane wave (vector amplitude $\mathbf{E}_0$, wavelength λ, wave number $k = 2\pi/\lambda$, and wave vector $\mathbf{k}_0$) propagating along the z-axis and incident on a spherical scatterer located in the origin (Figs. 1 and 2). Consider an observer in the xz-plane (scattering plane) with the scattering angle θ describing the angular deviation from the forward-scattering direction. Thus, the phase angle is $A = \pi - \theta$. In order to obtain the scattering characteristics for incident unpolarized light, the scattering problem needs to be solved for two perpendicular linear polarization states of the incident field, that is, for the y-polarized incident polarization vector perpendicular to the scattering plane and for the x-polarized incident polarization vector parallel to the scattering plane. The final scattering characteristics follow as the average of the characteristics for the two polarization states of the incident wave. To further simplify the illustration, consider the internal fields induced in the spherical particle on the x and y-axes only. In reality, interference can take place at differing depths in the direction of the z-axis and the depths do not need to be equal among the pairs of locations shown in Figs. 1 and 2. Assume, for the time being, that the six contributions depicted in Figs. 1 and 2 do not interfere with each other.

First, consider an incident electric field polarized parallel to the y-axis corresponding to the perpendicular polarization state. On the x-axis (Fig. 1(a)), due to the symmetry of the particle, the incident wave gives rise only to internal-field components ($\mathbf{E}_1$ and $\mathbf{E}_2$ with subscripts refering to the two dipoles) perpendicular to the scattering plane, that is, a y-polarized internal field. Such an internal field gives rise only to a y-polarized or positively polarized scattered field in the xz-plane. Contributions to the scattered field from two mirror locations a distance d apart on the x-axis ($x > 0$ and $x < 0$) interfere constructively in the exact backward direction; whereas, the interference varies from constructive to destructive in other directions in the xz-plane. On the y-axis, due to the spherical symmetry, the incident y-polarized wave gives rise to both y-polarized (Fig. 1(b)) and z-polarized internal-field components (Fig. 1(c)). The z-components at the mirror locations of the y-axis ($y > 0$ and $y < 0$) have opposite signs but are otherwise equal. Because the phase difference equals π, the scattered field components arising from the z-components cancel each other. Note that, in the backward and forward directions, no contribution can results from the z-polarized internal fields because there is no radiation along the line defined by the

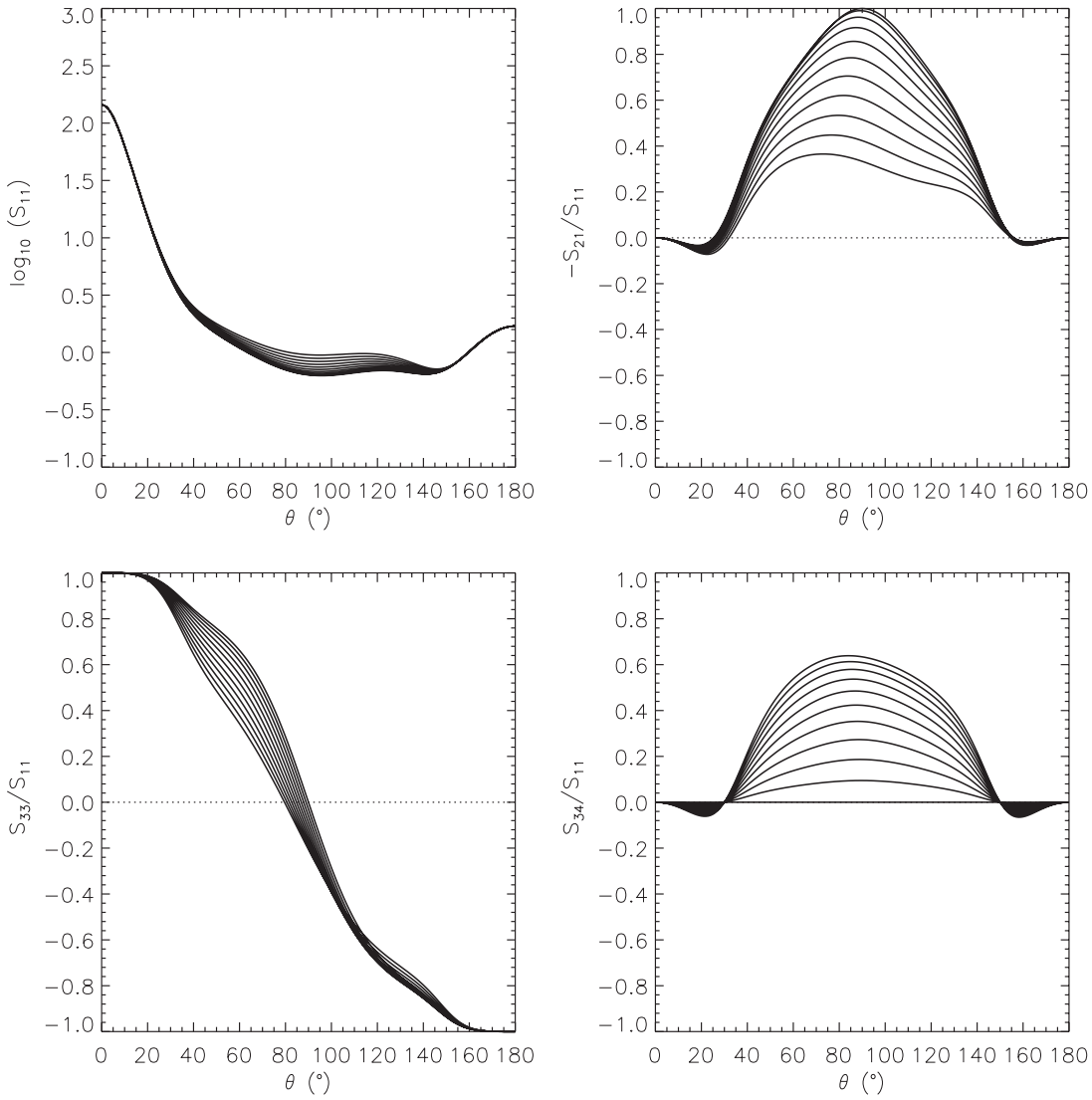

Fig. 3. Example analytical scattering-matrix elements using the present parameterization: $w = 0.8$, $g_1 = 0.8$, $g_2 = -0.2$, $w_1 = 0.5$, $a_t = 1$, $a_l = 0.0, 0.1, \ldots, 1.0$, $kd_1 = 2\pi$, $kd_2 = \frac{3}{2}\pi$, $kd_3 = \pi$, and $\phi_t - \phi_l = \frac{9}{10}\pi$.

electric field vector of an electric dipole scatterer. The y-components on the two sides are equal and result in scattered wave components that interfere constructively for all scattering angles in the xz-plane.

Second, consider an incident electric field polarized parallel to the x-axis corresponding to the parallel polarization state. On the x-axis, due to the spherical symmetry, the incident x-polarized wave gives rise to both x-polarized (Fig. 2(a)) and z-polarized (Fig. 2(b)) internal-field components. The z-components at the two mirror locations of the x-axis ($x > 0$ and $x < 0$) have opposite signs but are otherwise equal, thus having a phase difference of π. The scattered-field components arising from the z-components typically interfere non-destructively with one another, giving rise to negative polarization across the entire scattering-angle regime except the exact backward and forward scattering directions where, again, no contribution follows from the z-components of the internal fields. On the y-axis (Fig. 2(c)), due to the spherical symmetry, the incident wave gives rise only to an x-polarized internal-field component. The x-components at the two mirror locations ($y > 0$ and $y < 0$) are equal and result in scattered wave components that interfere constructively for all scattering angles with zero contribution for the scattering angle of $\pi/2$.

The single-scattering mechanism is based on the hypothesis that, typically, for the incident y-polarized field, the y-polarized internal-field components on the x-axis are stronger than those on the y-axis and, similarly for the incident x-polarized field, the x-polarized internal-field components on the y-axis are stronger than those on the x-axis. As a net result close to backscattering, with the x-polarized internal-field components on the y-axis predominating over other contributions via constructive interference, the degree of linear polarization for incident unpolarized light assumes negative values. This is enhanced by the first destructive interference geometry close to backscattering for the y-polarized scattered field arising from the x-axis. For both incident polarizations, the transverse internal-field components give rise to constructively interfering scattered-field components in the backward-scattering direction, resulting in a backscattering peak in the scattered intensity.

The single-scattering mechanism differs from the

coherent-backscattering mechanism. In coherent backscattering, reciprocal waves travel through the same scatterers in a random medium, interfering constructively in the exact backscattering direction but not necessarily in other directions. In the single-scattering mechanism, the electric fields on the mirror locations describe the net result of all possible interactions among the electric dipoles constituting the scatterer. Last but not least, coherent backscattering is typically seen to occur in supermicron length scales; whereas, the single-scattering mechanism is relevant in submicron-to-micron length scales for visible light.

The single-scattering mechanism has been verified for homogeneous spheres and Gaussian random particles by Tyynelä *et al.* (2007, 2008).

3. Scattering Parameterization

In what follows, we develop an analytical parameterization based on the scattering from pairs of electric dipoles. We make use of Figs. 1 and 2 in developing the amplitude scattering matrix elements and, in particular, fix the scattering plane to be the xz-plane. We follow the geometries in Figs. 1 and 2 and assume that the dipoles are located either on the y-axis (scatterer 1) or on the x-axis (scatterer 2). Treated separately, these scatterers produce pure scattering matrices and well-defined complex amplitude-scattering matrices. We assess two perpendicular polarization states of the incident wave propagating in the positive direction of the z-axis. Our present modeling relies on the differing interference characteristics along the x-axis for the perpendicular and parallel polarizations.

Let us start by studying scatterer 1 constituting a system in the direction of the y-axis (Figs. 1(b), 1(c), and 2(c)). Due to destructive interference, there is no contribution from the configuration in Fig. 1(c) in the scattering plane. Thus, the configuration in Fig. 1(b) is solely responsible for the contribution from the incident field perpendicular to the scattering plane. The configuration in Fig. 2(c) is solely responsible for the contribution from the incident field parallel to the scattering plane.

The amplitude scattering matrix is of a form identical to that of a Rayleigh particle:

$$\begin{aligned} S_1 &= 2a_t \exp(\mathrm{i}\phi_t), \\ S_2 &= 2a_t \exp(\mathrm{i}\phi_t)\cos\theta, \\ S_3 &= S_4 = 0, \end{aligned} \tag{1}$$

where a_t and ϕ_t are the amplitude and phase, respectively. Note, in particular, that there is no dependence on the distances between the dipoles.

The Mueller scattering matrix coincides with that of the Rayleigh case and is independent of the absolute phase ϕ_t:

$$\begin{aligned} S_{11} &= 2a_t^2\left(1+\cos^2\theta\right), \\ S_{12} &= 2a_t^2\left(-1+\cos^2\theta\right), \\ S_{21} &= S_{12}, \\ S_{22} &= S_{11}, \\ S_{33} &= 4a_t^2\cos\theta, \\ S_{44} &= S_{33}, \end{aligned} \tag{2}$$

the other elements being equal to zero.

Let us continue by studying scatterer 2, constituting a system in the direction of the x-axis (Figs. 1(a), 2(a), and 2(b)). The configuration in Fig. 1(a) is responsible solely for the contribution from the incident field perpendicular to the scattering plane. However, the contributions from configurations in Figs. 2(a) and 2(b) interfere with each other. For scatterer 2, we introduce the interdipole distances d_1, d_2, and d_3 corresponding to the configurations in Figs. 1(a), 2(a), and 2(b). Also, we assign different amplitudes and phase factors a_t, ϕ_t and a_l, ϕ_l for the transverse (Figs. 1(a) and 2(a)) and longitudinal (Fig. 2(b)) electric dipoles, respectively.

The amplitude scattering matrix takes the following form for scatterer 2:

$$\begin{aligned} S_1 &= 2a_t \exp(\mathrm{i}\phi_t)\cos\left(\frac{1}{2}kd_1\sin\theta\right), \\ S_2 &= 2a_t \exp(\mathrm{i}\phi_t)\cos\theta\cos\left(\frac{1}{2}kd_2\sin\theta\right) \\ &\quad + \mathrm{i}\,2a_l \exp(\mathrm{i}\phi_l)\sin\theta\sin\left(\frac{1}{2}kd_3\sin\theta\right), \\ S_3 &= S_4 = 0. \end{aligned} \tag{3}$$

The Mueller scattering matrix follows from the amplitude matrix and is more complicated than that for scatterer 1:

$$\begin{aligned} S_{11} &= 2a_t^2\cos^2\left(\frac{1}{2}kd_1\sin\theta\right) + 2a_t^2\cos^2\theta\cos^2\left(\frac{1}{2}kd_2\sin\theta\right) \\ &\quad + 2a_l^2\sin^2\theta\sin^2\left(\frac{1}{2}kd_3\sin\theta\right) \\ &\quad + 4a_t a_l\cos\theta\sin\theta\cos\left(\frac{1}{2}kd_2\sin\theta\right)\sin\left(\frac{1}{2}kd_3\sin\theta\right) \\ &\quad \cdot\sin(\phi_t-\phi_l), \\ S_{12} &= -2a_t^2\cos^2\left(\frac{1}{2}kd_1\sin\theta\right) + 2a_t^2\cos^2\theta\cos^2\left(\frac{1}{2}kd_2\sin\theta\right) \\ &\quad + 2a_l^2\sin^2\theta\sin^2\left(\frac{1}{2}kd_3\sin\theta\right) \\ &\quad + 4a_t a_l\cos\theta\sin\theta\cos\left(\frac{1}{2}kd_2\sin\theta\right)\sin\left(\frac{1}{2}kd_3\sin\theta\right) \\ &\quad \cdot\sin(\phi_t-\phi_l), \\ S_{21} &= S_{12}, \\ S_{22} &= S_{11}, \\ S_{33} &= 4a_t^2\cos\theta\cos\left(\frac{1}{2}kd_1\sin\theta\right)\cos\left(\frac{1}{2}kd_2\sin\theta\right) \\ &\quad + 4a_t a_l\sin\theta\cos\left(\frac{1}{2}kd_1\sin\theta\right)\sin\left(\frac{1}{2}kd_3\sin\theta\right) \\ &\quad \cdot\sin\left(\phi_t-\phi_l\right), \\ S_{34} &= 4a_t a_l\sin\theta\cos\left(\frac{1}{2}kd_1\sin\theta\right)\sin\left(\frac{1}{2}kd_3\sin\theta\right) \\ &\quad \cdot\cos(\phi_t-\phi_l), \\ S_{43} &= -S_{34}, \\ S_{44} &= S_{33}, \end{aligned} \tag{4}$$

the other elements being equal to zero. Scatterer 2 introduces the possibility for a nonzero S_{34}-element, a clear de-

viation from the pure Rayleigh behavior of scatterer 1. Note that we have deliberately decided not to introduce different z-coordinates for the configurations in Figs. 2(a) and 2(b). Such a difference would introduce additional phase differences that are left for a future study.

We define the average single-scattering matrix as a weighted sum of those for the scatterers 1 and 2, multiplied by a function that allows us to obtain reasonable single-scattering phase functions:

$$\boldsymbol{S} = f(\theta)\,[w_1\boldsymbol{S}_1 + (1-w_1)\boldsymbol{S}_2]\,, \tag{5}$$

where w_1 is the normalized weight of scatterer 1, $1-w_1$ is the normalized weight of scatterer 2, and $\boldsymbol{S}_1$ and $\boldsymbol{S}_2$ are the scattering matrices of scatterers 1 and 2, respectively. For the function $f(\theta)$, we incorporate the double Henyey-Greenstein (2HG) phase function

$$f(\theta) = w\frac{1-g_1^2}{\left(1+g_1^2-2g_1\cos\theta\right)^{\frac{3}{2}}} + (1-w)\,\frac{1-g_2^2}{\left(1+g_2^2-2g_2\cos\theta\right)^{\frac{3}{2}}},$$
$$g = wg_1 + (1-w)g_2$$

where g_1 and g_2 describe the forward and backward asymmetries, w is the normalized weight of the first Henyey-Greenstein function, and g is the asymmetry parameter of the full 2HG phase function. Note that, with the present multiplicative procedure, g is no longer the asymmetry parameter of the total scattering phase function. An alternative way to introduce the 2HG dependence is to make $f(\theta)$ contain in its denominator the S_{11} element of the combined scattering matrix of scatterers 1 and 2. The multiplication would then leave the pure 2HG function as the total scattering phase function. By choosing not to introduce the denominator, we are here conserving interference structures in the 11-element, too. For example scattering matrices, see Fig. 3.

4. Coherent-backscattering Simulations

We carry out example coherent-backscattering simulations for infinitely thick spherical random media of scatterers with the parameters indicated in Fig. 3 (choosing $a_l = 0.8$) for three single-scattering albedos $\tilde{\omega} = 0.3$, 0.6, and 0.9, and 28 extinction mean free paths $k\ell = 30$, 40, ... , 100, 120, 140, ... , 200, 250, 300, ... , 400, 500, 600, ... , 1000, 2000, 3000, ... , 5000, and 10000 (cf., Boehnhardt *et al.*, 2004; Muinonen, 2004). For $\tilde{\omega} = 0.3$ and 0.6, we sampled 100000 incident rays; whereas, for $\tilde{\omega} = 0.9$, we sampled 25000 rays due to extensive computational time.

Figure 4 shows the photometric and polarimetric phase functions for the spherical media for a number of mean free paths ($k\ell = 100$, 300, and 1000). Here ζ is the enhancement factor compared to the pure radiative-transfer contribution at the exact backscattering direction (e.g., Muinonen, 2004), and $P = (I_\perp - I_\parallel)/(I_\perp + I_\parallel)$ is the degree of linear polarization for unpolarized incident light (the subscripts refering to the intensity components perpendicular and parallel to the scattering plane). The single-scattering characteristics are seen to be neutralized and coherent backscattering gives rise to sharp photometric and polarimetric surges

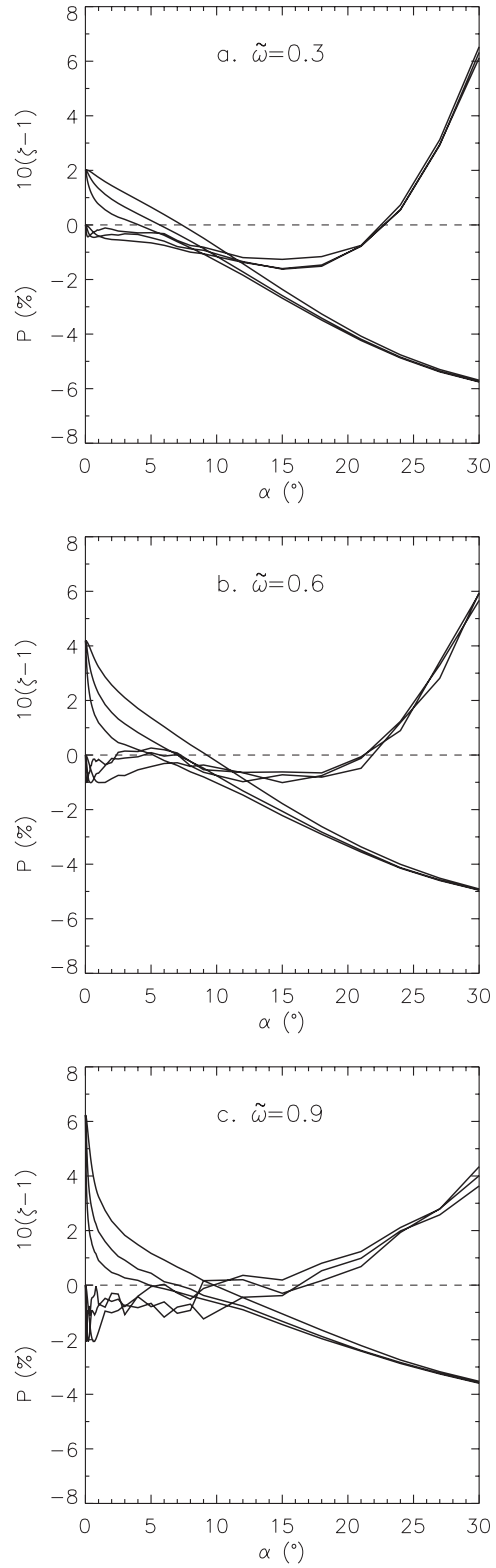

Fig. 4. Example coherent-backscattering results for spherical random media of infinite optical thickness.

close to the backscattering direction. A double-minimum feature appears for $\tilde{\omega} = 0.6$ in Fig. 4(b): it is straightforward to identify the negative coherent-backscattering and single-scattering lobes in the polarization curve. Note that, for $\tilde{\omega} = 0.9$, the single-scattering lobe disappears due to the dominating role of multiple scattering.

5. Conclusion

We have succeeded in developing an analytical semiempirical representation of amplitude and Mueller scattering matrices to be utilized in inverse problems concerning asteroid photometric and polarimetric phase curves. Our first numerical coherent-backscattering simulations show that the parameterization is realistic and flexible, allowing systematic application to the existing asteroid phase-curve data. Whereas we presently account for the differing interference characteristics along the x-axis for the perpendicular and parallel polarizations, it remains as our future goal to study analytically more complicated systems, such as those composed of four dipoles.

Acknowledgments. Research supported, in part, by the Academy of Finland (project No. 127461) and by the Chancellor at the University of Helsinki.

References

Boehnhardt, H., S. Bagnulo, K. Muinonen, M. A. Barucci, L. Kolokolova, E. Dotto, and G. P. Tozzi, Surface characterization of 28978 Ixion (2001 KX_{76}), *Astron. Astrophys.*, **415**, L21–L25, 2004.

Lumme, K. and J. Rahola, Comparison of light scattering by stochastically rough spheres, best-fit spheroids and spheres, *J. Quan. Spec. Rad. Trans.*, **60**, 439–450, 1998.

Muinonen, K., Coherent backscattering of light by complex random media of spherical scatterers: Numerical solution, *Waves Random Media*, **14**(3), 365–388, 2004.

Muinonen, K. and H. Erkkilä, Scattering of light by concave-hull-transformed Gaussian particles, in *Tenth Conference on Electromagnetic & Light Scattering*, edited by G. Videen, M. Mishchenko, M. P. Mengüc, and N. Zakharova, 125–128, (Bodrum, Turkey, June 17–22, 2007), 2007.

Muinonen, K., E. Zubko, J. Tyynelä, Yu. G. Shkuratov, and G. Videen, Light scattering by Gaussian random particles with discrete-dipole approximation, *J. Quan. Spec. Rad. Trans.*, **106**, 360–377, 2007a.

Muinonen, K., J. Tyynelä, E. Zubko, G. Videen, and Yu. G. Shkuratov, Single-scattering mechanism for negative polarization and opposition brightening of atmosphereless solar-system objects, in *39th Division for Planetary Sciences Meeting (DPS)*, Abstract, *BAAS*, **39**(3), 429 (30.05), 2007b.

Shkuratov, Y. G., A. Ovcharenko, E. Zubko, H. Volten, O. Munoz, and G. Videen, The negative polarization of light scattered from particulate surfaces and of independently scattering particles, *J. Quan. Spec. Rad. Tran.*, **88**, 267–284, 2004.

Tyynelä, J., E. Zubko, G. Videen, and K. Muinonen, Interrelating angular scattering characteristics to internal electric fields for wavelength-scale spherical particles, *J. Quan. Spec. Rad. Trans.*, **106**, 520–534, 2007.

Tyynelä, J., K. Muinonen, E. Zubko, and G. Videen, Interrelating scattering characteristics to internal electric fields for Gaussian-random-sphere particles, *J. Quan. Spec. Rad. Trans.*, **109**, 2207–2218, 2008.

Zubko, E., Yu. Shkuratov, K. Muinonen, and G. Videen, Collective effects by agglomerated debris particles in the backscatter, *J. Quan. Spec. Rad. Trans.*, **100**(1–3), 489–495, 2006a.

Zubko, E., Yu. G. Shkuratov, G. Videen, and K. Muinonen, Effects of interference on the backscattering properties of irregularly shaped particles using DDA, in *9th Conference on Electromagnetic and Light Scattering by Nonspherical Particles: Theory, Measurements, and Applications, Book of Abstracts*, edited by N. Voshchinnikov, 287–290, (St. Petersburg, Russia, June 5–9, 2006), 2006b.

Zubko, E., K. Muinonen, Yu. G. Shkuratov, G. Videen, and T. Nousiainen, Scattering of light by roughened Gaussian random particles, *J. Quan. Spec. Rad. Trans.*, **106**, 604–615, 2007.

K. Muinonen (e-mail: karri.muinonen@helsinki.fi), J. Tyynelä, E. Zubko, and G. Videen